Title
The spatial arrangement of the L and M cones in the central fovea of the living human eye

Journal
Vision Research, 38(17)

ISSN
0042-6989

Authors
Gowdy, Peter D
Cicerone, Carol M

Publication Date
1998-09-01

DOI
10.1016/s0042-6989(97)00416-1

PERGAMON

Vision Research 38 (1998) 2575–2589

Vision Research

The spatial arrangement of the L and M cones in the central fovea of the living human eye

Peter D. Gowdy [1], Carol M. Cicerone *

Department of Cognitive Sciences, University of California, Irvine, Irvine CA 92697, USA

Received 24 April 1997; received in revised form 23 October 1997

Abstract

Experiments designed to estimate the placement of L and M cones in fovea centralis of the living human eye are presented. Hyperacuity performances for two observers were measured for the full and the separate L and M cone submosaics using 2-dot chromatic stimuli on cone-selective adapting backgrounds. Simulated performances, based on an ideal observer model, were generated for all possible mosaics by varying L and M cone relative numerosity and spatial configuration. The best match between the simulated and measured performances determined the solution mosaic. Each observer's solution mosaic contained more L than M cones, randomly arrayed as assessed by statistical tests. © 1998 Elsevier Science Ltd. All rights reserved.

Keywords: Cone; Fovea; Topography; Hyperacuity; Photoreceptor

1. Introduction

1.1. Background

There is good agreement that in the primate retina the cone photoreceptors are placed in a hexagonal arrangement[2] [1–6] with the degree of hexagonal regularity decreasing as retinal eccentricity increases [1,4,6,7]. The long-wavelength sensitive (L), middle-wavelength sensitive (M), and short-wavelength sensitive (S) submosaics are interleaved to compose the hexagonal packing of the full cone mosaic. The way in which these three submosaics are interleaved is likely to have consequences for spectral and spatial sampling across the visual scene. There are at least three general schemes by which a particular cone type might be placed within the overall photoreceptor mosaic: First, clumping of a particular cone type can result in high spatial and spectral sampling within its clumped regions and poorer sampling elsewhere. Second, a uniformly-dispersed, regular arrangement of a cone type results in uniform but coarser spectral and spatial sampling. In this case, fixational eye movements may improve sampling in the fovea where cone spacing is small [5] but not in the peripheral retina where the spacing is larger [5]. Third, a random (homogeneous and isotropic) distribution represents a compromise between clumped and regular distributions in the sense that regions of aggregation and dispersion of like-type cones can occur by chance in random arrays.

The placement of the S cones is well established for both human [7–9] and non-human primates [10–12]. The consensus is that S cone placement in the peripheral retina shows only small deviations from a regular array and that S cones represent no more than 10% of the cone population at any eccentricity, except at the foveolar slope where they may reach a maximum of about 15% [9]. There is some disagreement about the presence [9] or absence [7,8] of S cones in the human central fovea and about the exact location and magnitude of the annular ring of highest S cone density. A sparse array may be an appropriate distribution scheme for the S cones because in the short-wavelength range

* Corresponding author. Fax: +1 949 8242307; e-mail cciceron@uci.edu.

[1] Present address: Department of Psychology, Harvard University, Cambridge, MA 02138, USA.

[2] Gauss [89] proved, based on the work of Lagrange [88], that a hexagonal lattice of non-overlapping, equal-area circles results in the maximum possible coverage of the 2D plane. The proportion of the total area covered by non-overlapping, equal-area circles placed according to a hexagonal lattice is $\pi\sqrt{3}/6$, or about 0.907, as compared to $\pi/4$, or about 0.785, for a square lattice.

PII: S0042-6989(97)00416-1

(< 500 nm), over which the S cones are most sensitive, chromatic aberration blurs the retinal image [13]. Furthermore, for the sparse S cone array a regular placement may be optimal because it minimizes gaps in spectral sampling as compared to a clumped or a random array; if a cone type is represented in good number, there is less need for regularity as a means for adequate spectral sampling across the visual scene.

In non-human primate retina mixed results have been reported for L and M cones. In baboon Marc and Sperling [10] used biochemical techniques to conclude that M cones are more numerous than L cones and their placements are random. Mollon and Bowmaker [14], using microspectrophotometry in talopoin retina, found equal numbers of L and M cones and a random distribution. More recently, Packer et al. [15], using photopigment transmittance imaging, concluded that the macaque retina contains roughly equal numbers of L and M cones, each arranged in clumps of like-type cones.

Psychophysical estimates of the relative numbers of the L and M cones indicate that there are more L cones as compared to M cones in the human retina [16–21] and that the relative numbers of L and M cones remains stable with eccentricity [22,23].

In this paper, the spatial arrangement of the L and M cones in the central fovea of the living human eye is estimated for two observers. Hyperacuity performances were measured for the full and the separate L and M cone submosaics using 2-dot chromatic stimuli on cone-selective adapting backgrounds. An ideal observer based analysis, stemming from the work of Geisler [24,25] and Geisler and Davila [26], was then developed and used to derive the underlying submosaics of L and M cones. It is concluded that in the human central fovea the L and M cones are randomly interleaved within the full cone mosaic. A brief report of this work has been previously presented [27].

1.2. General approach

Diffraction limitations of the pupil and image blurring due to the optics of the human eye [28] prevent the illumination of single cones in the center of the fovea where the cone-cone separation is estimated to be approximately 30 sec of arc [3,5,29]. To circumvent this obstacle a hyperacuity paradigm was used to take advantage of the fact that foveal hyperacuity thresholds are significantly smaller than the diameter of a single foveal cone [30–32]. Under the expectation that the contribution of a single foveal cone may have measurable effects on hyperacuity performance, comparisons of hyperacuity performance based on the full cone mosaic and on selected submosaics were used to reveal the placement of individual cones in the densely packed photoreceptor array of central fovea.

Only L or M cones were assumed to mediate the hyperacuity task for the following reasons. First, rods are known to be absent from within the central 21 min of arc of the fovea [5,29]. Second, in fovea centralis S cones are reported to comprise at most 3–5% of the cones [9] and may be totally absent [7,8]. Chromatic, 2-dot hyperacuity stimuli, superimposed on chromatic, cone-selective adapting background fields, were presented in central fovea. The wavelength of the hyperacuity stimulus was selected to favor detection by one cone type, and the wavelength of the adapting background was chosen to preferentially reduce the sensitivity of the other cone type e.g., [33]. For example, for L cone mediation of the hyperacuity task, long-wavelength hyperacuity stimuli were presented upon a middle-wavelength adapting background field.

Fig. 1 illustrates hypothetical hyperacuity performances based on the full cone mosaic, on the L cone submosaic, and on the M cone submosaic. As shown in Fig. 1, if hyperacuity performance is based on a fully tiled, hexagonal mosaic of cones, the results should trace out a smooth curve because the expected density of cones is about the same at all test presentation locations. Furthermore, performance should become progressively better with increasing offsets. On the other hand, under conditions in which a reduced mosaic mediates the task, when the stimulus falls in a gap there should be a reduction in hyperacuity performance corresponding to that location as compared to performance based on the full mosaic. In addition, performance based on the more numerous cone type should be better, on average, than that based on the more sparsely distributed type.

Hyperacuity is likely to be cortical in origin [34–39]. In order to link cone density to hyperacuity performance, an adaptation of Geisler's [24] ideal observer model was used. This model accurately predicts most aspects of human hyperacuity performance given only the information content of the stimulus and preneural factors of the human eye [24–26]. The model used in this study assumes an idealized, hexagonal packing geometry of the foveal cone mosaic, perfect fixational accuracy, and the optical scatter profile of the human eye [28]. Experimental evidence that there are only minor departures from hexagonal cone placement in central fovea will be reviewed in Section 5. Fixational accuracy for a well-practiced human observer is known to be excellent, with standard deviations on the order of a minute of arc [36,39]. As reviewed below, the impact of fixational inaccuracy exceeding these small values was evaluated in this study and found not to affect the analysis unless standard deviations were more than double these reported values. Simulations of hyperacuity performances based on the separate L and M cone submosaics were generated by the model for all possible relative numbers and spatial configurations of the L

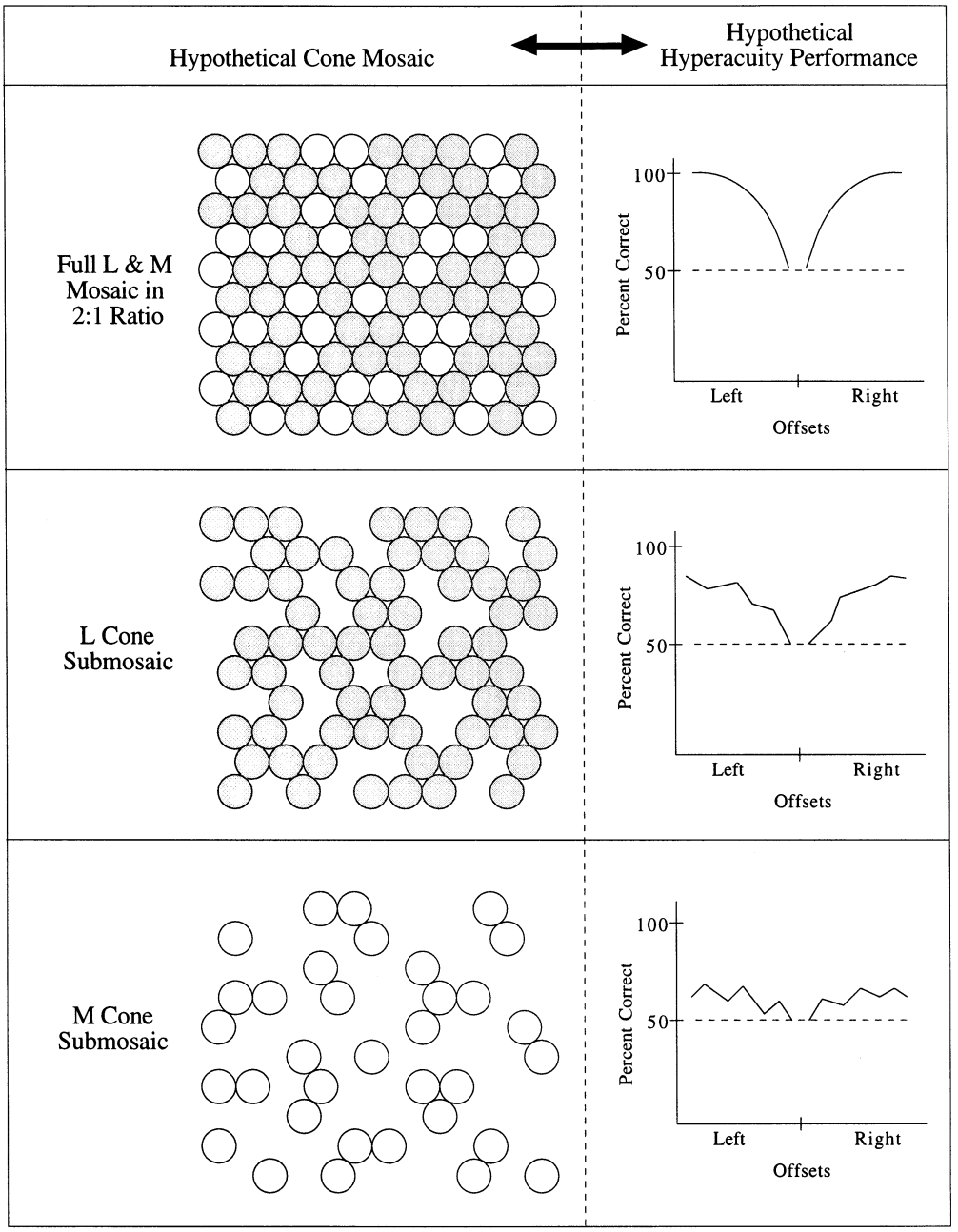

Fig. 1. TOP: A hypothetical cone mosaic composed of two L cones for each M cone in a random array (left) and its associated hypothetical hyperacuity performance (right) are illustrated. MIDDLE: The L cone submosaic (left) and the hypothetical hyperacuity performance based on it (right) are shown. BOTTOM: The M cone submosaic (left) and its associated performance (right) are also shown. As illustrated here, an increase in the number of detecting cones should produce an overall increase in hyperacuity performance. Also, hyperacuity performance based on submosaics (middle and bottom) may show irregularities if there are gaps in the submosaic.

and M cones in the test region. The best match between the simulated hyperacuity performance and the human observer's measured hyperacuity performance determined the solution mosaic.

Hyperacuity performance based on a single class of cones, either L or M, is essential for this analysis. The cone-selective adapting backgrounds which reduced the performance of one cone type, but not the other, to chance was determined in Section 2. Using the backgrounds derived in Section 2, hyperacuity performances based on the L cones, the M cones, or the full cone mosaic (with stimulus contrast equated in all conditions) were measured for two observers in Section 3. The ideal observer based analysis was then used to derive the L and M cone submosaics that best accounted for the cone-selective hyperacuity results of Section 3.

2. Experiment 1: Choice of the cone-selective adapting backgrounds

To obtain hyperacuity performances based on the separate L and M cone submosaics, adapting backgrounds which selectively reduced the performance of each cone type to chance were chosen. To this end we used the well known dependence of hyperacuity performance on contrast [34,37,40–43]. A fixed intensity hyperacuity test of 560 nm, selected for its near equal effectiveness for both the L and M cones [44], was presented upon a 560 nm background of variable intensity to produce contrasts ranging between 15–100%. The results indicated that hyperacuity performance was reduced to chance for stimuli of contrast $\leq 20\%$. As added confirmation, other results showed that a 620 nm hyperacuity test upon the chosen 620 nm background (L cone contrast of 14%) and a 520 nm hyperacuity test upon the chosen 520 nm background (M cone contrast of 14%) produced chance performance. Spectral sensitivity measurements provided additional verification that upon the 620 nm background of choice, M cones determined thresholds for middle-wavelength tests and that upon the 520 nm background of choice, L cones determined thresholds for long-wavelength tests.

2.1. Methods

2.1.1. Observers

The observer was PG (male, age 32 years). Anomaloscope (Neitz OT) matches, in addition to the Farnsworth–Munsell 100-hue test and Ishihara color plates, confirmed that he was color normal. Contact lenses corrected PG's mild myopia (-2.75D).

2.1.2. Apparatus

Fig. 2 illustrates the design of the two channel apparatus (top) and the stimulus display as seen by the observer (bottom). The hyperacuity stimuli were generated on a DECStation 5000/200 workstation and displayed on a Sony monitor (GDM-1960). The x- and y-chromaticity coordinates of the monitor's red, green, and blue phosphors were measured to be (0.61, 0.35), (0.28, 0.60), and (0.14, 0.05), respectively. The monitor was viewed at a distance of 36.25 feet. From that distance one pixel subtended 5 sec of arc. All stimuli displayed on the computer monitor were at full intensity white; wavelength and intensity were modified by the use of interference and neutral density filters as noted below. A separate channel and light source provided the backgrounds. The observer's head was fixed by means of a bitebar and the stimuli were monocularly viewed with the dominant eye through a 2.8 mm artificial pupil. A trial lens (-0.25D) was used to further increase the clarity of the stimuli. The bitebar and all optical components were securely fastened to an optical table. Energy calibrations were made with a Photo Research SpectraColorimeter (Model PR-650).

2.1.3. Stimuli

The hyperacuity stimulus consisted of two, vertically oriented squares (1 min of arc on a side). The stimulus components were separated vertically by 3 min of arc, chosen to be within the separation range of 2–5 min of arc in which 2-dot hyperacuity thresholds are known to be lowest [30–32]. To be near equally effective for both the L and M cones, the test wavelength was chosen to be 560 nm [44]. A test wavelength of 520 nm was selected to be preferentially effective for the M cones and a test wavelength of 620 nm was selected to be preferentially effective for the L cones. On any given trial the target (bottom) square was offset, relative to the fixed reference (top) square, to the left ($-$) or to the right

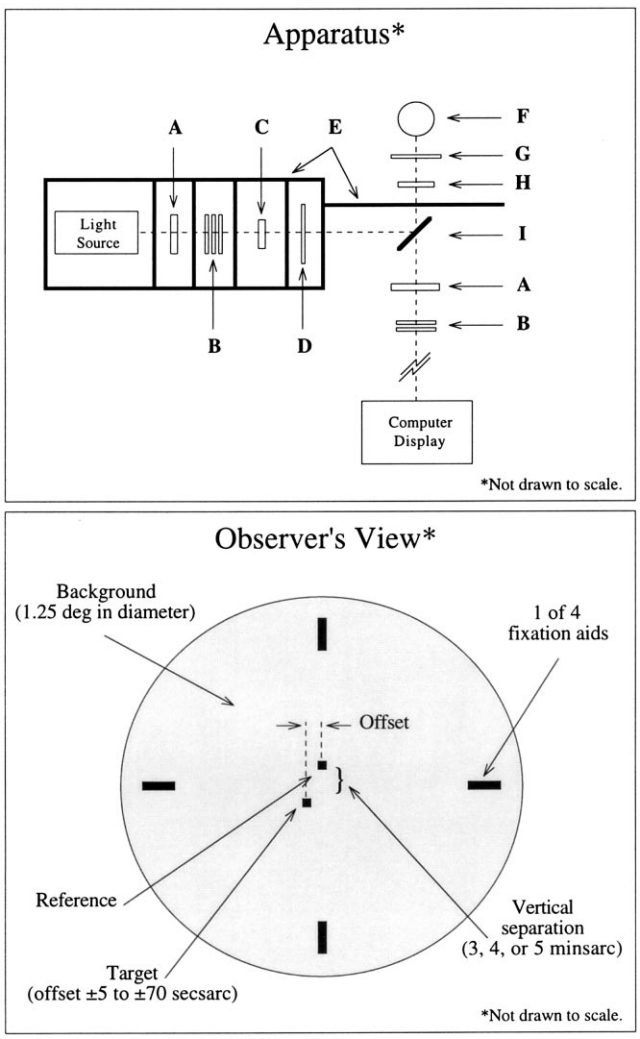

Fig. 2. TOP: A sketch of the two channel apparatus with interference filters (A), neutral density filters (B), diffusing glass (C), aperture (D), shielding (E), observer's eye (F), 2.8 mm artificial pupil (G), trial lens (H), and pellicle beam splitter (I). BOTTOM: A representation of the stimulus display as seen by the observers.

(+) by 5, 15, 25, 40, or 70 sec of arc. Presentations were made in pseudo-random order with the constraint that the same offset location could not be presented three or more times in consecutive order.

Continuously presented, small rectangular (1 × 4 min of arc) fixation aids were located at the end points of an imaginary cross. The center of fixation was at the midpoint of the vertical separation between the target and reference squares. The wavelength composition and luminance of the fixation aids were identical to the wavelength composition and luminance of the hyperacuity stimulus. The innermost edges of the four fixation lights was at least 20 min of arc beyond the stimulus components, well beyond the range where spatial interference is a factor [35]. Control experiments confirmed that (1) the orientation of the fixation aids (horizontal-vertical vs. diagonal) had no differential effect on hyperacuity performance, and (2) hyperacuity performance was better when the fixation aids were always present than when they were removed immediately prior to each stimulus presentation.

2.1.4. Background field

The diameter of the circular, continuously presented background field subtended 1.25°. For the full cone mosaic condition, a 560 nm background was used; for the L cone condition, a 620 nm background; and for the M cone condition, a 520 nm background. The intensity of the 560 nm test was held constant while the intensity of the 560 nm background field was varied to produce a test/background Michelson contrast, calculated in terms of cone excitation [45], of 100% (background absent), 73, 50, 27, 20, or 15%. The intensities of the 620 nm and 520 nm backgrounds were set to produce a test/background contrast of 14% for the L and M cones, respectively.

2.1.5. Procedure

To suppress microsaccades the observer was told that accurate fixation was extremely important [46,47]. Stimuli were self-presented, and the sessions were self-paced. The observer dark adapted for 15 min and then light adapted to one of the background fields for 5 min. When sure of accurate fixation, the observer presented the stimulus (via computer keyboard) which was flashed for a duration of 200 ms. The observer then responded (via computer keyboard) whether the target dot appeared to be offset to the right or to the left of the reference dot.

Each experimental session consisted of six blocks of trials. Each block corresponded to one of the six contrast conditions. The order of blocks was randomly determined from session to session. Each block consisted of 30 trials for each of ten offset locations: ±5, ±15, ±25, ±40, and ±70 sec of arc. The results are based on four experimental sessions (120 trials per offset location per contrast block).

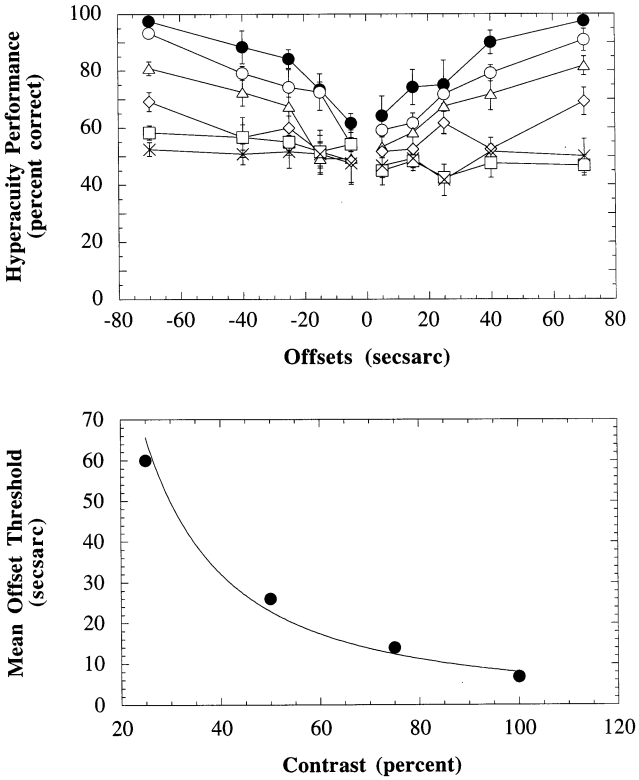

Fig. 3. TOP: Hyperacuity measurements based on the full cone mosaic as a function of target offset (−70 to 70 s of arc) for stimulus contrasts ranging between 15 and 100% are shown for observer PG. Results for the 100, 73, 50, 27, 20, and 15% contrast conditions are shown as filled circles, open circles, triangles, diamonds, squares, and crosses, respectively. Error bars represent one S.E.M. (between sessions). BOTTOM: PG's hyperacuity thresholds (65% correct) as a function of stimulus contrast are shown. The solid curve represents the best fitting power function as described in the text.

To reduce hyperacuity thresholds to a stable level, the observer practiced in the 100% contrast condition (with auditory feedback) for at least 5,000 trials prior to data collection [48,49]. After performance had reached a stable plateau, the final 100 trials at each offset location constituted data for this condition. Feedback was not provided during data collection.

2.2. Result

Hyperacuity performances for the 560 nm test upon a 560 nm background (referred to as the full cone mosaic condition) for contrasts of 100, 73, 50, 27, 20, and 15% are shown in Fig. 3 (top). Hyperacuity performance is near chance at all offset locations for contrasts of 15 and 20% and then improves steadily as contrast increases to 100%. Using a criterion of 65% correct, appropriate for the test luminance used in these experiments [42,50], PG's threshold measured at 100% contrast is approximately 7 sec of arc. This estimate is within the foveal hyperacuity range and in satisfactory agreement with threshold estimates reported in the literature for 2-dot stimuli [30–32].

Hyperacuity offset threshold (defined as the mean of the left and right threshold for each offset) is plotted as a function of percent contrast at the bottom of Fig. 3. The relationship between offset threshold (t) and percent contrast (c) is well described ($R^2 = 0.997$) by a power function of the form:

$$t = kc^n, \quad (1)$$

where k is a constant and the exponent n has a value of -1.52. This value of the exponent is within the range reported for different observers in previous studies of the effects of contrast on hyperacuity thresholds [34,37,40–43].

In order to confirm that test/background combinations producing $\leq 20\%$ contrast resulted in chance performance, we next measured hyperacuity performance under two conditions. In the first, a 620 nm hyperacuity test (for which L cone sensitivity exceeds M cone sensitivity by 0.69 log unit) was presented upon a 620 nm background, producing 14% contrast for the L cones. In the second, a 520 nm hyperacuity test (for which M cone sensitivity exceeds L cone sensitivity by 0.11 log) was presented upon a 520 nm background, producing M cone contrast of 14%. These measurements, shown in Fig. 4, confirmed that a choice of 14% contrast reduced hyperacuity performance based on the separate L and M cone mosaics to chance. Spectral sensitivity measurements provided additional verification that thresholds for long-wavelength tests were determined by L cones upon the 520 nm background of choice and that thresholds for middle-wavelength tests were determined by the M cones upon the 620 nm background of choice. Hence, hyperacuity performance is likely to be mediated by the M cones when the 520 nm test is superimposed upon the 620 nm background (referred to as the M cone condition) and by the L cones when the 620 nm test is superimposed upon the 520 nm background (referred to as the L cone condition).

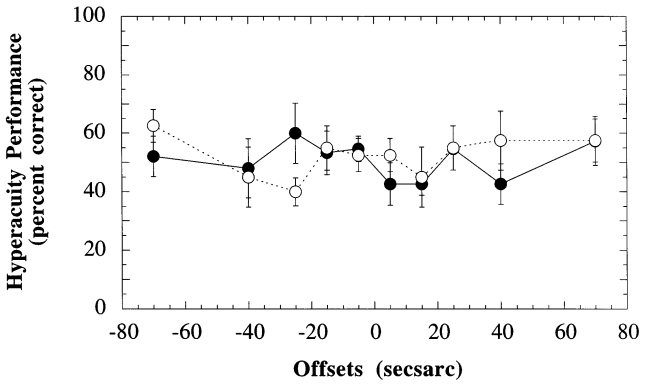

Fig. 4. Shown are PG's performances for the 620/620 (filled circles) and 520/520 (open circles) conditions for each of which contrast was set at 14%.

3. Experiment 2: Hyperacuity performance based on the L or M cone submosaics

Hyperacuity performance was measured for conditions in which either the L cones, the M cones, or both the L and M cones were likely to contribute to the task. For hyperacuity measurements based on L cones (620 nm test on a 520 nm background) or based on M cones (520 nm test on a 620 nm background), the contrast for the selected cone type was set to be approximately 50% while the contrast for the unselected cone type was set to approximately 14%, a value that reduced performance to chance levels as established in Section 2. For hyperacuity based on both the L and M cones (560 nm test on a 560 nm background) contrast was 50% for both cone types. In addition to measurements made at 50% contrast, the results of Section 2 measured at 100% contrast for the full cone array (560 nm stimulus, no background) provided a reference for the effects of reduced contrast on hyperacuity performance.

3.1. Methods

3.1.1. Observers

In addition to PG, two emmetropes (EL, female, age 24 years and RB, male, age 21 years), neither of whom were aware of the purposes of the experiment, served as observers. Anomaloscope (Neitz OT) matches in addition to the Farnsworth–Munsell 100-hue test and Ishihara color plates indicated that both EL and RB were color normal. Full analysis of PG's and EL's results are presented. The results from RB showed the same general trends as PG's and EL's but were highly variable from day to day even after practice.

3.1.2. Apparatus

The apparatus and stimuli were identical to those described in Section 2.1.2.

The dimensions and offset locations of the stimuli and the fixation aids were identical to those used in Experiment 1 with the following exceptions. A separation of 3 min of arc between the target and reference dots was used for observers EL and RB. For observer PG three different vertical separations, 3, 4, and 5 min of arc, were used. By using different separations, all within the range where foveal hyperacuity thresholds are reported to be lowest [29–31], hyperacuity measurements could be collected over a larger extent of central fovea. In order to determine the set of cones illuminated for each separation between the reference and target dots, the optical scatter profile of the human eye [28] was convolved with the target dot. It was assumed that a minimum of six quanta was necessary to activate a cone [19,20,51]. As can be seen in Fig. 5, the strips of effectively illuminated cones (shaded circles) corre-

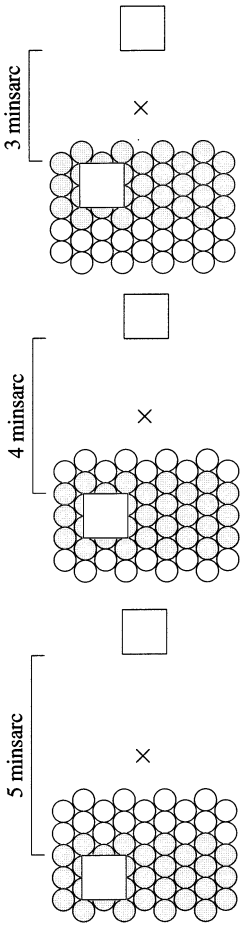

Fig. 5. Shown are schematic illustrations of the strips of cones illuminated for different separations of the two components of the hyperacuity stimuli. The reference (open square, top) and target (open square, bottom), offset to the left relative to the reference, are shown in each panel. Shaded circles represent the set of cones (strip) effectively illuminated by the target as offset location is varied between ± 70 sec of arc for separations of 3 min of arc (left panel), 4 min of arc (middle panel), and 5 min of arc (right panel). The small cross at the center of each panel (not present in the actual stimulus display) marks the center of fixation.

sponding to different separations are partially overlapping.

Chromatic aberrations due to the differing wavelength compositions of the hyperacuity stimuli and backgrounds are minimal for the wavelengths used here. Furthermore, hyperacuity performance is not affected appreciably by moderate degrees of blur [52,53]. Nonetheless, trial lens corrections for optical clarity were tested. The two emmetropic observers did not use any corrections. The myope (PG) used a trial lens (-0.25) in all experiments.

3.1.3. Cone-selective adapting background fields

The M cone and L cone conditions were designed to measure M cone based and L cone based hyperacuity performance, respectively. The combination of the 520 test upon the 620 background provided 50% contrast for the L cones and 14% contrast for the M cones. The combination of the 620 test upon the 520 background provided 50% contrast for the M cones and 14% contrast for the L cones. The full cone condition, providing 50% contrast for L and M cones, was used to gauge the effects of contrast alone for performance based on a full mosaic of cones. For the full cone mosaic, only the 100% contrast condition was run for EL and RB because of their limited availability.

3.1.4. Procedure

The procedures were identical to those described in Section 2.1.5 with the following exceptions. There were ten daily experimental sessions, each consisting of three (for PG) or two (for EL and RB) blocks. One of the conditions, randomly chosen, was run in each block. Each block consisted of ten stimulus presentation trials at each of the ten target offset locations for each of the target-reference separations (300 trials for PG and 100 trials for EL and RB).

3.1.5. Correction for response bias

In this analysis hyperacuity performance is linked to the number of cones in the underlying cone array. In order to remove any confounding effects of response bias, we applied a correction to each observer's results as follows: Response bias, independent of the effects of cone density, was assessed using the results for the full cone condition at 100 or 50% contrast for which the full complement of cones contributed to performance. The response bias correction, c, was calculated for each offset location as:

$$c = -0.5[z(H) + z(F)], \quad (2)$$

where $z(H)$ and $z(F)$ are the z-scores for the hit and false alarm rates, respectively [54]. A small left bias of 0.045 ± 0.012 was shown by PG in the full cone condition for 50% contrast and a similar left bias of 0.038 ± 0.013 for 100% contrast. A small left bias of 0.073 ± 0.042 was shown by EL in the full cone condition for 100% contrast.

3.2. Results

The hyperacuity results of PG are shown in Fig. 6. The hyperacuity performances for the different separations in the full mosaic, 100% contrast condition were not significantly different, as expected due to nearly constant cone density in this small region of central fovea [5]. Therefore, the same full mosaic, 100% contrast function, averaged over separations, is shown. Even without the ideal observer analysis (presented in Section 4), a number of qualitative inferences can be drawn from a comparison of the hyperacuity performances under the different conditions shown in Fig. 6.

Performance was generally better when based on the L cones than when based on the M cones at all target-reference separations, suggesting a greater number of L cones as compared to M cones as explained in Section 1.2 and illustrated in Fig. 1. For a separation of 3 min of arc (Fig. 6, top), there is a greater difference between the L- and M-cone-based performances for right offsets as compared to left offsets, suggesting a greater numerosity of L cones as compared to M cones in the region underlying the offsets to the right as compared to the region underlying the offsets to the left.

The hyperacuity performance based on L cones, M cones, and the full cone mosaic for observer EL with the 3 min of arc separation are shown in Fig. 7. The results from EL show that hyperacuity performance based on the L cones is better than that based on the M cones, consistent with a greater number of L cones as compared to M cones. The smaller difference between her L and M cone measurements as compared to the difference in PG's results suggest an overall L to M cone ratio closer to unity for EL. Furthermore, EL's results suggest that there is a high concentration of M cones underlying the far right offsets, as indicated by her better performance based on M cones as compared to L cones there.

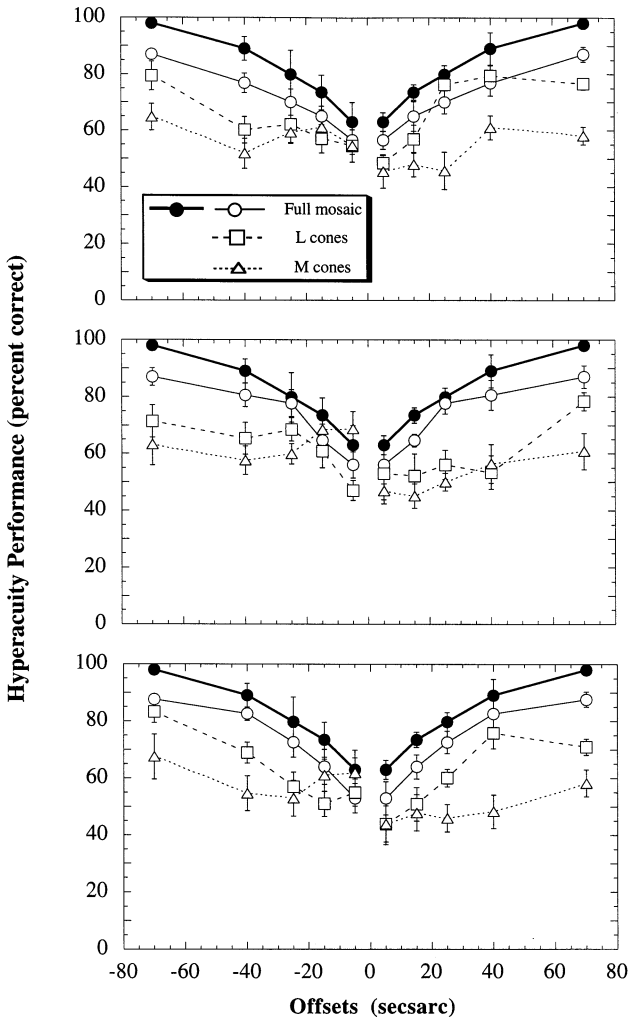

Fig. 6. Shown are PG's hyperacuity measurements for the 3 (top), 4 (middle), and 5 (bottom) min of arc separations between the target and reference for four test/background conditions: the two full cone conditions one at 100% contrast (filled circles, thick lines) and the other at 50% contrast (open circles, thin lines), the L cone condition (50% contrast, open squares, dashed lines), and the M cone condition (50% contrast, open triangles, dotted lines). Error bars represent one S.E.M.

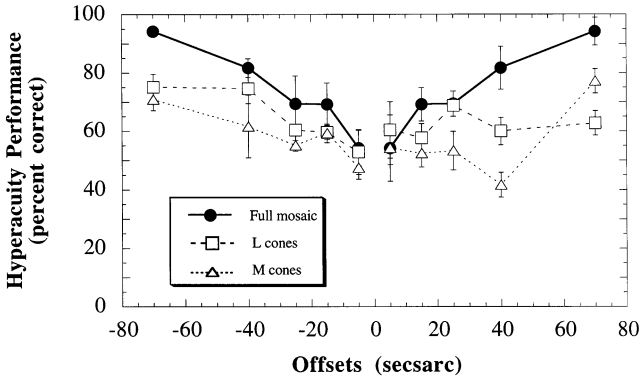

Fig. 7. Hyperacuity measurements for observer EL are shown for the full cone, L cone, and M cone conditions with a 3 min of arc separation between target and reference components of the hyperacuity test stimulus. Symbols are as in Fig. 6.

4. Ideal observer based analysis

In this section, an ideal observer model based on the work of Geisler [24] is described and used to determine the cone mosaic most likely to have produced the results obtained in Section 3. This model was chosen because it accurately predicts most aspects of human hyperacuity performance and is applicable near threshold [25,26]. As described in detail below, the model takes into account the dimensions of the stimuli, the mean number of photons delivered, the optical quality of the human eye, the photoreceptor sampling array, photoreceptor optics (size, shape, wave-guide properties), and photoreceptor spectral sensitivities. In addition, the model assumed that fixation was exact from trial to trial. This assumption is reasonable based on the following: First, human fixational accuracy, limited by the combined effects of eye tremor and drift [55–57], is reported to have a S.D. near 1 min of arc [36,39,58]. Second, variability in fixational accuracy was minimized by the use of fixation aids and briefly flashed, self-presented stimuli. Third, analyses conducted in this study show that a S.D. of fixational accuracy ≤ 2 min of arc does not significantly affect our ideal observer based analysis, producing negligible changes (within measurement error) in simulated per-

formance. The cone mosaic most likely to account for each observer's hyperacuity data was selected by comparing the observer's performance to the model's simulated hyperacuity performance for all possible mosaics consisting of different numbers and spatial configurations of the L and M cones.

4.1. Model

The model calculates a measure of discriminability, d', between % a comparison stimulus, α, and a target stimulus, β:

$$d' = \frac{\sum_{i=1}^{n} (\beta_i - \alpha_i) \ln\left(\frac{\beta_i}{\alpha_i}\right)}{\sqrt{0.5 \sum_{i=1}^{n} (\beta_i + \alpha_i) \ln^2\left(\frac{\beta_i}{\alpha_i}\right)}} \quad (3)$$

where α_i and β_i are the expected numbers of effectively absorbed quanta in the i^{th} receptor due to α and β, respectively.

The ideal observer convolved the target with a functional expression [26] for the optical scatter profile of the human eye for a 3 mm pupil [28]. The ideal observer assumed a perfect hexagonal lattice of circular (cross-section) cones with center-to-center spacing of 30 sec of arc and an effective circular integration aperture of 20 sec of arc in diameter for each cone [2,3,6,9,59–61]. Two prototypical mosaic orientations, vertical and 30° rotated from vertical, were examined. A rotation of 30° was chosen because it is the midpoint between a vertical orientation and a 60° rotation which would produce cone placements identical to that of a vertically oriented mosaic.

4.2. Selection of α and the relationship between performance and d'

Experiment 2 conforms to what Macmillan and Creelman [54] refer to as a classification experiment in which the proper discrimination statistic is the cumulative d' for the n^{th} stimulus:

$$d'_n = \sum_{i=2}^{n} z[p_i] - z[p_{i-1}] \quad (4)$$

In Eq. (4), $z[p_i]$ is the z-score corresponding to the observer's proportion correct, p, for the stimulus at the i^{th} location.

To derive α in this analysis the observer's results based on the full cone mosaic were used to calculate cumulative d' values for each target offset location. The choice of α for the model was determined as that location which generated the best match between the d' values generated by the model as compared to data-based cumulative d' values. For observer PG, α values located at $+45$ sec of arc for left offsets and -45 for right offsets were chosen based on a chi-square analysis ($\chi^2 = 6.23$, $\upsilon = 29$, $p > 0.995$). For observer EL, α values located at ± 86 sec of arc were chosen ($\chi^2 = 9.80$, $\upsilon = 9$, $p > 0.25$).

A way in which to link model-calculated d' to simulated performance, expressed as percent correct, is required for this analysis. A function describing the correspondence between d' and performance can be derived for each observer by pairing the observer's performance for the full mosaic to the cumulative d' values, given that target offsets occurred with equal probability and response bias was corrected [54]. Fig. 8 plots PG's (top) and EL's (bottom) hyperacuity performance (percent correct) as a function of cumulative d'. The theoretical point (0, 50) links $d' = 0$ to chance performance. The results for all separations and offsets are plotted. A second degree polynomial function provides a good fit to PG's measurements ($R^2 = 0.964$). The dashed curve represents the relationship between the model's calculated d' values (Eq. (3)) and simulated performance for the choices of $\alpha = \pm 45$ sec of arc for PG. A second degree polynomial function also provides a good fit to EL's data ($R^2 = 0.939$). The dashed curve shows the relationship between the model's calculated

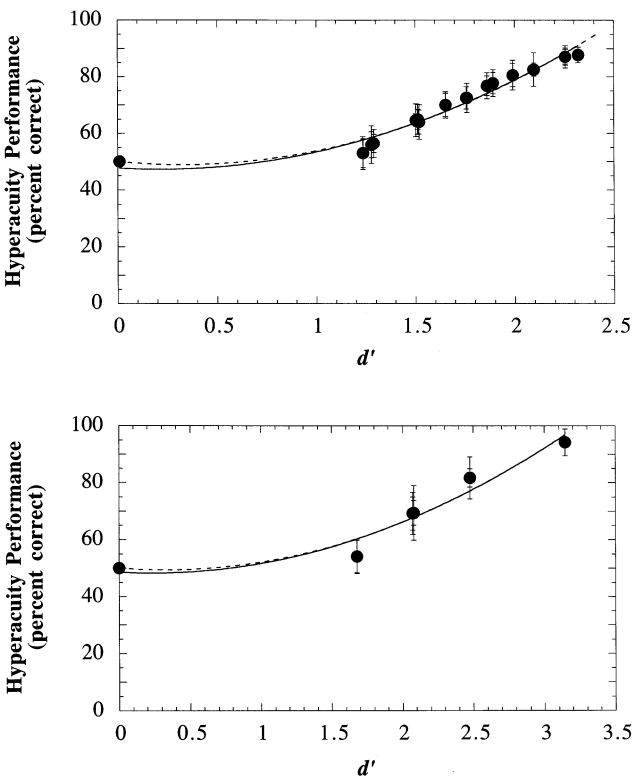

Fig. 8. TOP: Shown is a plot of PG's hyperacuity performance as a function of d' for the full cone, 50% contrast condition for all separations and offsets. The solid curve represents the best fitting second order polynomial. The dashed curve represents the relation between simulated performance by the model and d' with $\alpha = \pm$ 45 sec of arc. Error bars represent one S.E.M. BOTTOM: EL's full cone, 100% contrast hyperacuity performance as a function of d' for all offsets. Curves are as described above, except $\alpha = \pm 86$ sec of arc.

d' values and simulated performance when $\alpha = \pm 86$ s/arc for EL. The good agreement between the solid curves, the dashed curves, and hyperacuity data for both observers means that the model accurately predicts hyperacuity performance for the full mosaic under the conditions of this experiment. Assuming that equal d' values correspond to equal performance, this function allows us to link the model's calculation of d' to percent correct. We tested whether the hyperacuity performances as a function of d' based on the L cone submosaic and that based on the M cone submosaic could be described by the same function derived for the full mosaic. The functions shown in Fig. 8 for PG and EL accounted for 92.3 and 93.1%, respectively, of the variability in each observer's M cone and L cone results.

4.3. General procedure

The ideal observer first determined the set of cones to be included in the analysis for each target offset. Under the assumptions that a cone absorbs 27% of the incident quanta [62,63] and that six or more quantal absorptions (above the background) are required to activate a cone [19,20,51], a cone center located within 1.25 min of arc of the center of the target's scatter profile was included in the analysis (7–11 cones for the full mosaic).

Next, for each possible L and M cone mosaic, ranging from all L to all M, the ideal observer calculated (Eq. (3)) a d' value for the subset of L cones and a separate d' value for the subset of M cones using each observer's value of α. The ideal observer then converted the d' values to simulated L cone based or M cone based hyperacuity performances by means of the function (solid curves in Fig. 8) linking d' and percent correct. Chi-square values were calculated by comparing the observer's L- and M-cone-based performances to the simulated performances. The L and M cone mosaic that minimized the sum of these two chi-square values was chosen as the mosaic that best accounted for the observer's L cone based and M cone based hyperacuity results at that offset location (referred to as a local solution). This procedure was then repeated for all offset locations at all target-reference separations.

Given the small differences in offsets and the optical scatter profile of the human eye, it was possible for a single cone to contribute to performance at more than one offset location. Such a cone would be represented in more than one local solution and could be assigned as an L cone in some local solutions and as an M cone in others. All possible L and M assignments to all such contested cones were examined again. While holding the L and M assignments to the uncontested cones fixed, the set of assignments for contested cones which minimized chi-square values summed over all offsets and separations was determined. This procedure resulted in the selection of an overall solution mosaic of L and M cones that best accounted for the observer's measurements as a whole.

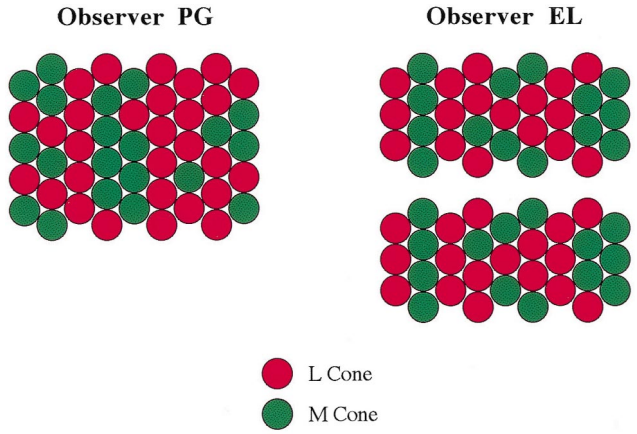

Fig. 9. Shown are the L and M cone mosaics that best account for observer PG's (left) and EL's (right) hyperacuity performance based on L or M cones. Red and green circles represent the locations of L and M cones, respectively. Two mosaic solutions for observer EL differ only in terms of a switch in the location of two cones (fourth column from the left). These two mosaics produce equivalent simulated performances (see text).

If two cone mosaics are mirror reversals about the horizontal axis they yield the same simulated hyperacuity performance; hence they are equivalent mosaics in terms of this analysis. Note that such mosaics do not differ in the relative numbers of L and M cones, but L and M cone placements may be mirror reversals about the horizontal axis.

4.4. Results

Fig. 9 illustrates overall solutions for PG and for EL. To allow a direct comparison of the mosaics to the observers' hyperacuity performances (Figs. 6 and 7), the mosaics have been reflected about the vertical and horizontal axes to account for the eye's optics. For both observers a vertical orientation of the mosaic resulted in smaller chi-square values as compared to a 30° rotated orientation. For observer PG a unique overall solution was found whereas for EL two equivalent solutions, differing in only one pair of switched cones, were found. The unique solution obtained for observer PG is likely explained by the added constraints in the analysis provided by overlapping strips.

Observer PG's L to M cone ratio for the mosaic shown in Fig. 9 is 1.45, and EL's ratio is 1.21. The estimate of PG's L to M cone ratio obtained in this analysis agrees with an independent, small-spot estimate of 1.4 for this observer and falls within the range previously reported in this lab [19,21,22]. Furthermore, based on a ratio of 1.45 a wavelength of 583 nm is

predicted to be judged uniquely yellow according to an analysis linking cone ratio to unique yellow in a sample of color normals [21]. The foveal unique yellow of PG is 584 nm, in good agreement with the predicted value. The estimate of 1.21 for EL's L to M cone ratio is slightly below the lowest value of 1.3 [23] obtained with small-spot detection techniques.

Fig. 10 shows the ideal observer's simulated performances (calculated for target offsets varying in steps of 1 sec of arc) based on the L and M cone submosaics shown in the overall solution mosaic for PG (Fig. 9). The simulated performances are compared to PG's measured L and M cone based hyperacuity performance for the 3 min of arc (top), 4 min of arc (middle), and 5 min of arc (bottom) separations. The simulated

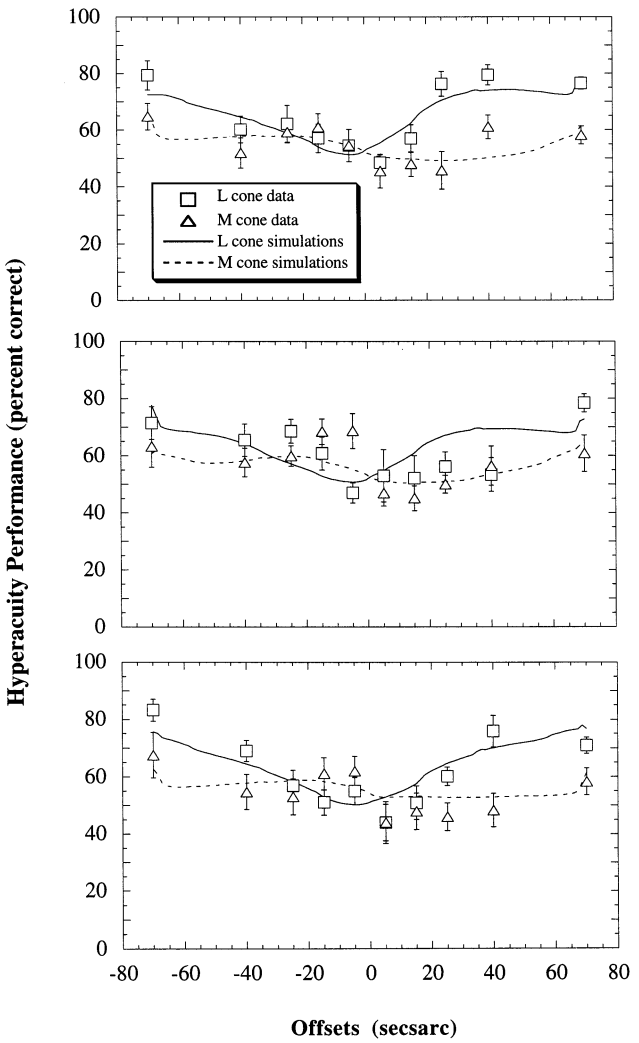

Fig. 10. The model's simulated performances based on PG's solution mosaic are shown for the 3 (top), 4 (middle), and 5 (bottom) min of arc target-reference separations (see Fig. 9). Solid and dashed lines represent the model's simulated performance (calculated in steps of 1 sec of arc) based on the L and M cone submosaic, respectively. Observer PG's hyperacuity measurements are shown for the L cone (open squares) and M cone (triangles) conditions. Error bars represent one S.E.M.

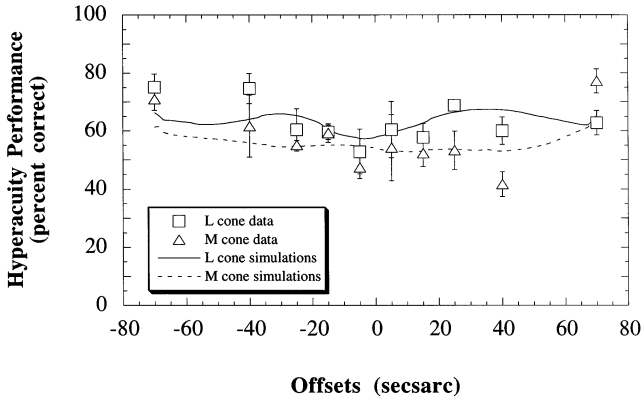

Fig. 11. The model's simulated performance based on EL's (equivalent) solution mosaics for the 3 min of arc target-reference separation is shown. Symbols and curves as in Fig. 10.

performance is not significantly different from PG's hyperacuity performance ($\chi^2 = 35.28$, $\upsilon = 29$, $p > 0.10$). Fig. 11 shows the ideal observer's simulated performances for the L and M cones in EL's solution mosaics as compared to her measured L and M cone based performances. Simulated performance is not significantly different from observer EL's performance ($\chi^2 = 12.66$, $\upsilon = 9$, $p > 0.10$).

4.5. Statistical analysis of mosaics

To determine the packing arrangement of the L and M cones in each observer's solution mosaic, Ripley's [64] L statistic (based on a frequency count of the distances of each cone to its nearest like-type neighbors) and a runs test [65] were employed. The L statistic was chosen for a number of reasons: It has been effectively used to assess S cone placement [66]; its minimum required sample size (seven) is smaller than the number of cones in each observer's mosaic; and it can distinguish among regular, clumped, and random arrays under the assumptions of homogeneity and isotropy which are likely to hold for the fovea. Simulations were conducted to confirm that the L statistic clearly distinguishes among regular (square and hexagonal), clumped, and random arrays of cones for sample sizes matching those of the present study. Toroidal edge correction was used as recommended by Ripley [64] for samples of this size. For each observer's analysis, the expected value and 95% confidence interval of the L statistic were calculated for a random distribution of cones based on 500 hexagonally-packed and vertically-oriented mosaics for which the L to M cone ratio equaled that of the observer's solution mosaic. (Pilot analyses determined that using more than 500 random mosaics does not significantly change the results of this test.) The evaluation of the L statistic for each observer's overall solution mosaic was then compared to these expected results. This comparison indicated that the

placements of L and M cones for both observers' overall solution mosaics fell well within the calculated 95% confidence interval for a random array but not for either regular or clumped arrays. Thus, the hypotheses of clumped or of regular arrays were rejected, whereas the hypothesis of a random array could not be rejected.

The L statistic cannot detect directionally biased nonrandom distribution patterns because of the assumption of isotropy. A casual inspection of Fig. 9 suggests there may be vertically oriented runs of like-type cones in the solution mosaics. Consequently, a nonparametric statistical test [65] was used to determine whether the number of observed L and M cone runs differs significantly from the expectations of grouping (runs) in a random pattern. If the number of runs along any cardinal direction of the hexagonal array is less than expected by chance then this is an indication of significant clumping. For a random grouping of m items of one type (e.g. M cones) and n items of the other type (e.g. L cones), $m \leq n$, the probability of $u \leq u'$ can be expressed as

$$P\{u \leq u'\} = \frac{1}{C_m^{m+n}} \sum_{u=2}^{u'} f_u, \tag{5}$$

where, $f_u = 2C_{k-1}^{m-1} \cdot C_{k-1}^{n-1}$ when $u = 2k$ and $f_u = C_{k-1}^{m-1} \cdot C_{k-2}^{n-1} + C_{k-2}^{m-1} \cdot C_{k-1}^{n-1}$, when $u = 2k-1$, for $k = 1, 2, \ldots, m+1$. Runs of cones (numbering ≥ 1) were counted in traverses along the three cardinal axes of the hexagonal mosaics of Fig. 9. Under the assumption that the distribution of the number of runs is approximately normal for $m, n \geq 10$ [65], the numbers of observed L and M cone runs in the solution mosaics of both observers were found not to differ significantly from the expectations of a random grouping along any cardinal axis (one-tailed test, $\alpha = 0.05$).

Hence, two different statistical tests, one directionally insensitive and the other directionally sensitive, indicate that the placements of the L and M cones in the tested foveal patches of two human observers do not differ from the expectations of random placements. Larger samples than those of the present study may better reflect any inhomogeneities across the retina and may reveal patterns of cone placement differing from random.

5. Discussion

In the present work hyperacuity performances based separately on the L cone submosaic, the M cone submosaic, and the full cone mosaic of the central fovea were measured. Simulations of hyperacuity performance based on an ideal observer analysis were used to obtain the L and M cone mosaic most likely to account for the hyperacuity measurements for two human observers. We conclude that the central foveal photoreceptor matrix is populated by more L than M cones and each cone class is randomly interleaved to comprise the full cone photoreceptor matrix.

5.1. Local departures from a hexagonal arrangement and S cones in the central foveal mosaic

For simplicity and computational tractability it was assumed that the central foveal mosaic consists of a hexagonal array of L and M cones. Under these assumptions, PG's hyperacuity performance for the 4 min of arc separation is not fully consistent with his results at the 3 and 5 min of arc separations. The inconsistency could be resolved if there were gaps in the cone mosaic which would result in poorer performance in one region as compared to nearby regions. Two plausible reasons for gaps in the L and M cone mosaic are local departures from a perfect hexagonal arrangement and the existence of S cones, in addition to L and M cones, in the central foveal array.

Some research suggests that the central fovea may be characterized by a small degree of local nonhexagonal packing [6,67,68] as well as unequal cone spacing along the horizontal as compared to the vertical meridian [3,6,69]. In particular, the work of Pum et al. [68] suggests that there are large (55 cones on average) 'foveal iso-orientation areas' that are hexagonal in shape and within which cones are placed in a hexagonal arrangement. The cone placements within different foveal iso-orientation areas are reported to differ slightly in terms of their internal axial orientation, and the borders between these areas are typically characterized by small departures from hexagonal placement, resulting in relatively larger local cone spacings.

An alternative explanation is that a small number of S cones may be present in this foveal region for observer PG. The presence of S cones would have the effect of introducing regions of decreased hyperacuity performance because the stimuli were chosen to be effective for the L and M cones and not the S cones. In support of this hypothesis, anatomical work in both human [9] and non-human primates [10] indicate that a small percentage ($\leq 5\%$) of central foveal photoreceptors may be S cones. However, other anatomical work in both monkey [11,12] and human retina [7] as well as psychophysical work in humans [8,70–72] indicate that the central fovea is free of S cones. The diameter of the S-cone-free zone has been estimated to range between 3.6 and 9 min of arc [11,12] in macaque retina whereas in humans the S cone-free zone is larger, about 20 min of arc in diameter [7]. Individual variability in the size of the S-cone-free area of central fovea may be the basis for these discrepant findings [7]. We tested whether the inclusion of S cones would improve the fit between the data and the model's simulated performance in PG's results. This analysis showed a small

improvement for a change in a single L cone to an S cone (on the right hand side within the 4 min of arc strip) with additional changes showing no improvement in the fit. Thus, our analysis is consistent with at most one S cone out of 49 cones, or roughly 2%, near the lower end of the range reported in the literature. The discrepancy between the hyperacuity performance for the 4 min of arc strip and performance for nearby areas cannot be completely explained by the presence of S cones. Therefore, our results tend to be compatible with the existence of some degree of local departures from hexagonal packing as well as a small number of S cones in the center of the human fovea.

5.2. Cross-species comparison of L and M cone relative numerosity and packing geometry

A numerical superiority of L cones as compared to M cones agrees with previous measurements in humans [16–22] but is inconsistent with the reverse finding in baboon [10] and the finding of roughly equal numbers in talopoin [14] and macaque [15]. The conclusion of random placement is in agreement with the results of Marc and Sperling [10] and Mollon and Bowmaker [14] for the non-human primate retina but not with the results of Packer et al. [15] who find clumping of like-type cones.

5.3. Consequences of various distribution schemes for the different cone classes

We suggest that a random distribution of cone types might represent a spatial and spectral sampling scheme that is a compromise between regular and clumped arrays of cones. A regular array is characterized by good chromatic sampling across the visual scene whereas the spatial resolution of each cone submosaic should be less good, especially in the peripheral retina. By comparison, a cone array with a high degree of clumping is characterized by poor chromatic sampling across the visual scene but with the possibility of increased cone-specific spatial resolution at the clumped locations. Random mosaics tend to be characterized by different patterns in different regions; by chance, there is some degree of clumping and some degree of dispersion among like-type cones.

If the L and M cones are interleaved in a regular array, a straight-forward expectation is that acuity based on the L or M cone submosaics should be worse than that based on the full mosaic. A number of studies based on grating stimuli [73,74] or laser interference fringes [75] show that the acuity based on either cone class alone is no poorer than that based on the full cone mosaic. If the array is regular, some sort of postreceptoral processing could exploit any correlations in the signals from the L and M cones in order to produce these results [76]. Alternatively, the cone mosaic may not be regular, in which case clumps of like-type cones may provide acuity measures for L or M cone submosaics that are equal to those based on the full mosaic.

Clumping is likely to be a poor scheme for producing color opponent receptive fields. There is good agreement that the centers of color opponent receptive fields in the fovea are fed by a single cone type [77–80] but there is some controversy as to whether their surrounds receive inputs from a single cone type [77,81–83] or mixed cone types [84–87]. In either case, clumping of cones would interfere with the formation of color-opponent receptive field surrounds in clumped regions because inputs to the surrounds from cone types different from those of the center must be drawn from distant retinal locations. On the other hand, either random or regular placements of cone types would ease the formation of color opponency [84,85,87].

A random placement of cone types does not preclude nonrandom connectivity; therefore, the results reported in this paper cannot resolve the issue of specific versus nonspecific L and M cone inputs to the surrounds of chromatically antagonistic receptive fields. However, a random scheme for the interleaving of the L and M cones may best provide for the dual requirements of color opponency and spatial resolution because random distributions tend to be characterized by regions of moderate clumping and other regions of near regularity.

Acknowledgements

This work was supported by grant EY11132 (PHS-NIH National Eye Institute) to CMC.

References

[1] Wässle H, Riemann HJ. The mosaic of nerve cells in the mammalian retina. Proc R Soc B (Lond) 1978;200:441–61.
[2] Williams DR. Aliasing in human foveal vision. Vis Res 1985;25:195–205.
[3] Williams DR. Topography of the foveal cone mosaic in the living human eye. Vis Res 1988;28:433–54.
[4] Hirsch J, Miller WH. Does cone positional disorder limit resolution? J Opt Soc Am A 1987;4:1481–92.
[5] Curcio CA, Sloan KR, Kalina RE, Hendrickson AE. Human photoreceptor topography. J Comp Neurol 1990;292:497–523.
[6] Curcio CA, Sloan KR. Packing geometry of human cone photoreceptors: variation with eccentricity and evidence for local anisotropy. Vis Neurosci 1992;9:169–80.
[7] Curcio CA, Allen KA, Sloan KR, Lerea CL, Hurley JB, Klock IB, Milam AH. Distribution and morphology of human cone photoreceptors stained with anti-blue opsin. J Comp Neurol 1991;312:610–24.
[8] Williams DR, MacLeod DIA, Hayhoe MM. Punctate sensitivity of the blue-sensitive mechanism. Vis Res 1981;21:1357–75.

[9] Ahnelt PK, Kolb H, Pflug R. Identification of a subtype of cone photoreceptor, likely to be blue sensitive, in the human retina. J Comp Neurol 1987;255:18–34.
[10] Marc RE, Sperling HG. Chromatic organization of primate cones. Science 1977;196:454–6.
[11] de Monasterio FM, Schein SJ, McCrane EP. Staining of blue-sensitive cones of the macaque retina by fluorescent dye. Science 1981;213:1278–81.
[12] Wikler KC, Rakic P. Distribution of photoreceptor subtypes in the retina of diurnal and nocturnal primates. J Neurosci 1990;10:3390–401.
[13] Yellott JI, Wandell BA, Cornsweet TN. The beginnings of visual perception: the retinal image and its initial encoding. In: Greiger SR, editor. Handbook of Physiology: The Nervous System III. Bethesda: American Physiological Society, 1984.
[14] Mollon JD, Bowmaker JK. The spatial arrangement of cones in the primate fovea. Nature 1992;360:677–9.
[15] Packer OS, Williams DR, Bensinger DG. Photopigment transmittance imaging of the primate photoreceptor mosaic. J Neurosci 1996;16:2251–60.
[16] de Vries HL. Luminosity curve of trichromats. Nature 1946;157:736–7.
[17] de Vries HL. The heredity of the relative numbers of red and green receptors in the human eye. Genetica 1948;24:199–212.
[18] Vos JJ, Walraven PL. On the derivation of the foveal receptor primaries. Vis Res 1970;11:799–818.
[19] Cicerone CM, Nerger JL. The relative numbers of long-wavelength-sensitive to middle-wavelength-sensitive cones in the human fovea centralis. Vis Res 1989;29:115–28.
[20] Vimal RLP, Pokorny J, Smith VC, Shevell SK. Foveal cone thresholds. Vis Res 1989;29:61–78.
[21] Cicerone CM. Color appearance and the cone mosaic in trichromacy and dichromacy. Proceedings of the symposium international research group on color vision deficiencies. Tokyo, Japan, 1990;1–12.
[22] Nerger JL, Cicerone CM. The ratio of L cones to M cones in the human parafoveal retina. Vis Res 1992;32:879–88.
[23] Cicerone CM, Otake S. Color-opponent sites: Individual variability and changes with retinal eccentricity. Investig Ophthalmol Vis Sci (Suppl) 1997;38:2130.
[24] Geisler WS. Physical limits of acuity and hyperacuity. J Opt Soc America A 1984;1:775–82.
[25] Geisler WS. Sequential ideal-observer analysis of visual discriminations. Psychol Rev 1989;96:267–314.
[26] Geisler WS, Davila KD. Ideal discriminators in spatial vision: two-point stimuli. J Opt Soc Am A 1985;2:1483–97.
[27] Gowdy PD, Cicerone CM. The spatial arrangement of L and M cones in central fovea of the living human eye. Opt Photonics News (Suppl) 1996;7:66.
[28] Campbell FW, Gubisch RW. Optical quality of the human eye. J Physiol 1966;186:558–78.
[29] Østerberg G. Topography of the layer of rods and cones in the human retina. Acta Ophthalmol (Suppl) 1935;6:1–103.
[30] Westheimer G, McKee SP. Spatial configurations for visual hyperacuity. Vis Res 1977;17:941–7.
[31] Westheimer G. The spatial grain of the perifoveal visual field. Vis Res 1982;22:157–62.
[32] Groll SL, Hirsch J. Two-dot vernier discrimination within 2.0 degrees of the foveal center. J Opt Soc Am A 1987;4:1535–42.
[33] Stiles WS. Mechanisms of colour vision. London: Academic Press, 1978.
[34] Watt RJ, Morgan MJ. The recognition and representation of edge blur: evidence for spatial primitives in human vision. Vis Res 1983;23:1465–77.
[35] Levi DM, Klein SA, Aitsebaomo AP. Vernier acuity, crowding and cortical magnification. Vis Res 1985;25:963–77.
[36] McKee SP, Levi DM. Dichoptic hyperacuity: the precision of nonius alignment. J Opt Soc Am A 1987;4:1104–8.
[37] Wilson HR. Responses of spatial mechanisms can explain hyperacuity. Vis Res 1986;26:453–69.
[38] Paradiso MA, Carney T, Freeman RD. Cortical processing of hyperacuity tasks. Vis Res 1989;29:247–54.
[39] Fahle M. Psychophysical measurements of eye drifts and tremor by dichoptic or monocular vernier acuity. Vis Res 1991;31:209–22.
[40] Klein SA, Casson E, Carney T. Vernier acuity as line and dipole detection. Vis Res 1990;30:1703–19.
[41] Waugh SJ, Levi DM. Visibility, timing and vernier acuity. Vis Res 1993;33:505–26.
[42] Waugh SJ, Levi DM. Visibility, luminance and vernier acuity. Vis Res 1993;33:527–38.
[43] Waugh SJ, Levi DM. Visibility and vernier acuity for separated targets. Vis Res 1993;33:539–52.
[44] Smith VC, Pokorny J. Spectral sensitivity of the foveal cone photopigments between 400 and 500 nm. Vis Res 1975;15:161–71.
[45] MacLeod DIA, Boynton RM. Chromaticity diagram showing cone excitation by stimuli of equal luminance. J Opt Soc Am 1979;69:1183–6.
[46] Steinman RM, Cunitz RJ, Timberlake GT, Herman M. Voluntary control of microsaccades during maintained monocular fixation. Science 1967;155:1577–9.
[47] Puckett JDW, Steinman RM. Tracking eye movements with and without saccadic correction. Vis Res 1969;9:695–703.
[48] Westheimer G, McKee SP. Stereoscopic acuity for moving retinal images. J Opt Soc Am 1978;68:450–5.
[49] Fahle M, Edelman S. Long-term learning in vernier acuity: effects of stimulus orientation, range and feedback. Vis Res 1993;33:397–412.
[50] Morgan MJ, Aiba TS. Vernier acuity predicted from changes in the light distribution of the retinal image. Spat Vis 1985;1:151–61.
[51] Marriott FHC. The foveal absolute visual threshold for short flashes and small fields. J Physiol Lond 1963;169:416–23.
[52] Stigmar G. Blurred visual stimuli II: The effect of blurred visual stimuli on vernier and stereo acuity. Acta Ophthalmol 1971;49:364–79.
[53] Toet A, Snippe HP, Koenderink JJ. Effects of blur and eccentricity on differential spatial displacement discrimination. Vis Res 1988;28:535–53.
[54] Macmillan NA, Creelman CD. Detection Theory: A User's Guide. Cambridge: Cambridge University Press, 1991.
[55] Riggs LA, Ratliff F. Visual acuity and the normal tremor of the eyes. Science 1951;114:17–8.
[56] Ditchburn RW, Ginsborg BL. Involuntary eye movements during fixation. J Physiol 1953;119:1–17.
[57] Ditchburn RW. Eye-movements in relation to retinal action. Optica Acta 1955;1:171–6.
[58] Riggs LA, Armington JC, Ratliff F. Motions of the retinal image during fixation. J Opt Soc Am 1954;44:315–21.
[59] Yamada E. Some structural features of the fovea centralis in the human retina. Arch Ophthalmol 1969;82:151–9.
[60] Miller WH, Bernard GD. Averaging over the foveal receptor aperture curtails aliasing. Vis Res 1983;23:1365–9.
[61] Curcio CA, Allen KA. Topography of ganglion cells in human retina. J Comp Neurol 1990;300:5–25.
[62] Schnapf JL, Kraft TW, Baylor DA. Spectral sensitivity of human cone photoreceptors. Nature 1987;325:439–41.
[63] Schnapf JL, Nunn BJ, Meister M, Baylor DA. Visual transduction in cones of the monkey Macaca fascicularis. J Physiol 1990;427:681–713.
[64] Ripley BD. Spatial Statistics. New York: Wiley, 1981.

[65] Swed FS, Eisenhart C. Tables for testing randomness of grouping in a sequence of alternatives. Ann Math Stat 1943;14:66–87.
[66] Shapiro MB, Schein SJ, de Monasterio FM. Regularity and structure of the spatial pattern of blue cones of macaque retina. J Am Stat Assoc 1985;80:803–12.
[67] Hirsch J, Curcio CA. The spatial resolution capacity of human foveal retina. Vis Res 1989;29:1095–101.
[68] Pum D, Ahnelt PK, Grasl M. Iso-orientation areas in the foveal cone mosaic. Vis Neurosci 1990;5:511–23.
[69] Coletta NJ, Williams DR. Psychophysical estimate of extrafoveal cone spacing. J Opt Soc Am A 1987;4:1503–13.
[70] Willmer EN. Color of small objects. Nature 1944;153:774–5.
[71] Wald G. Blue-blindness in the normal fovea. J Opt Soc Am 1967;57:1289–303.
[72] Castaño JA, Sperling H. Sensitivity of the blue-sensitive cones across the central retina. Vis Res 1982;22:661–73.
[73] Green DG. The contrast sensitivity of the colour mechanisms of the human eye. J Physiol 1968;196:415–29.
[74] Cavonius CR, Estevez O. Contrast sensitivity of individual colour mechanisms of human vision. J Physiol 1975;248:649–62.
[75] Williams DR. The invisible cone mosaic. Advances in Photoreception: Proceedings of a Symposium on Frontiers of Visual Science. Washington, DC: National Academy Press, 1990:135–48.
[76] Williams DR, Sekiguchi N, Haake W, Brainard D, Packer O. The cost of trichromacy for spatial vision. In: Valberg A, Lee BB, editors. From Pigments to Perception: Advances in Understanding Visual Processes. New York: Plenum Press, 1991.
[77] Wiesel TN, Hubel DH. Spatial and chromatic interactions in the lateral geniculate body of the Rhesus monkey. J Neurophysiol 1966;29:1115–56.
[78] Boycott BB, Dowling JE. Organization of the primate retina: light microscopy. Phil Trans Roy Soc, B 1969;255:109–84.
[79] Shapley R, Perry VH. Cat and monkey retinal ganglion cells and their visual functional roles. Trends Neurosci 1986;9:229–35.
[80] Boycott BB, Wässle H. Morphological classification of bipolar cells of the primate retina. Eur J Neurosci 1991;3:1069–88.
[81] Shapley R, Reid RC, Kaplan E. Receptive field structures of P and M cells in the monkey retina. In: Valberg A, Lee BB, editors. From Pigments to Perception: Advances in Understanding Visual Processes. New York: Plenum Press, 1991.
[82] Reid RC, Shapley RM. Spatial structure of cone inputs to receptive fields in primate lateral geniculate nucleus. Nature 1992;356:716–8.
[83] Masland RH. Unscrambling color vision. Science 1996;271:616–7.
[84] Paulus W, Kröger-Paulus A. A new concept of retinal colour coding. Vis Res 1983;23:529–40.
[85] Young RA, Marrocco RT. Predictions about chromatic receptive fields assuming random cone connections. J Theor Biol 1989;141:23–40.
[86] Lennie P, Haake PW, Williams DR. The design of chromatically opponent receptive fields. In: Landy MS, Movshon JA, editors. Computational Models of Visual Processing. Cambridge, MA: MIT Press, 1991.
[87] DeValois RL, DeValois KK. A multi-stage color model. Vis Res 1993;33:1053–65.
[88] Lagrange JL. Recherches d'arithmétique, Nouveaux Mémoires de l'Académie Royal des Sciences et Belles-Lettres de Berlin 1773.
[89] Gauss CF. Untersuchungen über die eigenschaften der positiven ternären quadratischen Formen von Ludwig August Seeber. Göttingische Gelehrte Anzeigen (July 9) 1831.